Int. Journ. of Wettability Science and Technology, Vol. 1, pp. 95–120
Reprints available directly from the publisher
Photocopying permitted by license only

Surface Engineering for the Control of Polyethylene Terephthalate (PET) Wettability Characteristics Using Laser Beam Wavelength

J. LAWRENCE[1,*], D.G. WAUGH[1], C.D. WALTON[2], N. LANGER[3] AND S. BIDAULT[3]

[1]*School of Mechanical, Aerospace and Automotive Engineering, Faculty of Engineering, Environment and Computing, Coventry University, Gulson Road, Coventry, CV1 2JH, UK*
[2]*School of Mathematics and Physical Sciences, University of Hull, Hull, HU6 7RX, UK*
[3]*DataPhysics Instruments GmbH, Raiffeisenstraße 34, 70794 Filderstadt, Germany*

The science and technology behind using laser beam wavelength and the subsequent manipulation of the polar component of the surface free energy of a material (through atmospheric oxygen content) to design and control the contact angle behaviour of the surface of polyethylene terephthalate (PET) is presented. The findings indicate that the theory will be applicable to most polymers. When exposed to infrared (IR) CO_2 laser irradiation the PET surface experienced no change in chemistry and, therefore, no change in polar component occurred. There was, however, topography change to produce a rougher surface; consequently, contact angle followed the Wenzel, *etc*. theories and increased, changing the surface from hydrophilic to hydrophobic. In contrast, ultraviolet (UV) KrF excimer laser beam radiation altered both the topography and chemistry of the PET surface. The very nature of processing polymers with UV laser radiation inherently generates a surface that is more oxygen-rich with enhanced functional groups, which cause an increase in its polar nature. This UV laser irradiation–induced enhanced polar nature has more of an effect than topography for polymers, which, in turn, effects a decrease in contact angle. In this instance the PET surface became more hydrophilic. There is now movement towards a new science-based platform from which to assess, research and establish the methodologies for wettability characteristics design and modification through controlled laser beam exposure.

Keywords: CO_2 laser, KrF excimer laser, Polyethylene terephthalate (PET), surface engineering, wettability, contact angle, functional groups, polar component

*Corresponding author: e-mail: jonathan.lawrence@coventry.ac.uk, jl-laserengineering@hotmail.com

1 INTRODUCTION

In many instances, the only way to meet the demand for relatively inexpensive and easy to engineer polymeric materials possessing surface properties appropriate for the intended application is through surface engineering. Industrial and academic sectors driving polymer surface engineering research activity are in printing [1] electronics [2, 3], food packaging [4, 5], biological tissue engineering [6-8], anti-bacterial barriers [9, 10], coating technologies [11, 12] and adhesion [13-15]. Certain applications mean that wettability plays the lead role in increasing the functionality of a surface. Greater understanding of the fundamentals of wettability characteristics have enabled researchers working in the field of surface treatment to modify the wettability characteristics of polymeric materials [16-24].

The low surface free energy and chemical inertness of polyethylene terephthalate (PET) gift it with poor adhesive bonding characteristics; consequently, it is very difficult to wet and, therefore, bond PET without surface engineering to enhance its wettability characteristics. Mechanical and flame methods, which essentially roughen the polymer surface to promote improved mechanical bonding, have been used, but these cause increased degradation and reduce mechanical strength [25]. Chemical treatments to primarily increase the surface oxygen content of various polymer materials have been used, but are often accompanied by an undesirable loss in strength. [26-28]. Plasma treatments have also shown a good deal of promise for polymer material surface modification [29-32], with many fold increases in the interfacial shear strength being occasioned after some plasma treatments. Hot embossing has also been demonstrated as a successful means for enhancing wettability characteristics [33]. Still, despite the very beneficial improvements in interfacial shear strength, the actual process itself is extremely complex and, consequently, somewhat difficult to control.

A point of considerable importance with all of these existing process is that they have a tendency to alter the bulk properties rather than just the uppermost surface layer. Lasers, on the other hand, can offer the user not only an exceedingly high degree of process controllability, but also a great deal of process flexibility.

Ultraviolet (UV) excimer laser radiation has been shown to be a very effective means of enhancing the wettability characteristics of polymer materials. Considerable research effort has been expended to study the effects of excimer laser radiation on the wettability characteristics of polyethylene PET in its many forms [33-35]. Breuer *et al.* [36] demonstrated that when processing with optimum excimer laser parameters, improvements in and control of the adhesion strength polypropylene (PP) films could be achieved. It was suggested that such improvements were the result of the excimer laser surface

engineering generating a more polar surface. This increased polarity of surfaces following excimer laser surface engineering was also reported by Laurens *et al.* [37, 38] in their work on polyether-etherketon (PEEK), adding that the choice of laser wavelength had a crucial influence on the resultant wettability characteristics of the PEEK. Song and Netravali [39-41] examined the effects of excimer laser radiation on the interfacial characteristics of UHSPE fibres and epoxy resin with a view increasing interfacial shear strength. Considerable increases in the interfacial shear strength were achieved and were ascribed to more favourable wettability characteristics through increased surface roughness, surface oxygen content and polar nature after excimer laser surface engineering. Using a femtosecond laser, Yoon *et al.* [42] produced a superhydrophobic surface on poly(dimethylsiloxane) (PDMS) by creating a roughened surface in the nanoscale and microscale to give topography akin to the Lotus leaf. Toosi *et al.* [43] presented a comprehensive review on state-of-the-art in excimer laser ablation of micropatterns and nanopatterns into the surfaces of polymers for wettability characteristics modification, and successfully used excimer laser beams to ablate the surface of polytetrafluoroethylene (PTFE) to produce surfaces with superhydrophobic behaviour [44].

Infrared (IR) lasers have been demonstrated as viable and flexible means of modifying the wettability characteristics of various polymers. Wettability characteristics have been modified by Waugh *et al.* [43-45] using a CO_2 laser beam to generate hydrophilic surfaces on nylon 6,6. The levels of accuracy and control obtained were sufficiently high that surfaces with bespoke levels of bioactivity were created. Khorasani *et al.* [46] used CO_2 laser radiation for surface modification of PDMS to produce superhydrophobic surfaces. These workers found that the laser treated surface contained carbonate groups which enriched the oxygen content and the hydrophobicity was found to be a function of the number of laser pulses. Many applications require hydrophobic and superhydrophobic surfaces, such as antibacterial barriers. Surfaces with controlled levels of hydrophilicity were CO_2 laser engineered onto food packaging PET films by Waugh and Lawrence [47] and Lawrence and Waugh [48], with the outcome being tailored surfaces that offered bacterial resistance. As a means of controlling the wettability and adhesion characteristics of polymers, both UV and IR lasers have been assessed for the laser surface engineering of polymethyl methacrylate (PMMA) [49], polyethylene (PE) [50], nylon 6,6 and PET [51]. These workers found that laser beam wavelength was a control parameter and with the correct selection of wavelength and process parameters, contact angle could be manipulated with high accuracy, resolution and repeatability. Later work by Waugh and Lawrence [52] refined the CO_2 laser engineering of PMMA for the modification of wettability characteristics through surface patterning.

The work described herein moves this current knowledge on to the next level by presenting a methodology for controlling the wettability characteristics of PET by surface engineering; thus allowing the design and production of surface characteristics tailored for specific applications. Laser beam wavelength and operating parameters selection are the means of control and the science and technology underpinning this work will be applicable to most polymers. The controlled surface engineering of the PET was achieved using a CO_2 laser and a KrF excimer laser. Analytical techniques were employed to determine the topography and chemistry of the surface of the PET before and after laser beam interaction. It was found that laser surface engineering caused the contact angle to follow the established theories of Wenzel, *etc.*; however, this was wavelength dependant. The governing effect of surface oxygen content on the polar component of the surface free energy of the PET was identified as a processing parameter.

2 EXPERIMENTAL DETAILS

2.1 Laser surface engineering procedure

2.1.1 Material specification and sample preparation

PET films (Goodfellow, Ltd.), biaxially oriented and of 0.25 mm thickness were used for the experimentation. Samples were cut into 10×15 cm^2 billets for experimental purposes. Prior to laser surface engineering the films were cleaned in acetone and then in ethanol for three minutes each at room temperature then dried in a sample drier for a minimum of an hour.

2.1.2 CO_2 laser surface engineering methodology

The CO_2 laser used was a 60 W CO_2 laser system (Firestar; Synrad, Inc.) including a galvanometric scanning head. This CO_2 laser emitted a Gaussian beam at 10.6 μm in the continuous wave (CW) mode. In order to create the desired pattern upon the PET film surface Synrad Winmark Pro software (Synrad, Inc.) was used to scan the laser beam within a square working field of 110×110 mm^2. The experimental billets were then secured down with a bracket and positioned at the focal point which was 190 mm away from the surface of the sample to the focussing lens on the galvanometric head. All samples were treated in ambient air and an extraction system was used to remove any fumes produced during the laser processing.

Constant laser parameters were used for all patterns produced. The power was set to 10.0% (6 W), the transverse scanning speed was set to 400 mm/s and the spot size was maintained at 95 μm. Sample sets of two different track and two different hatch patterns were produced: tracks with 350 and 400 μm spacing between each line were used to create the different CO_2 laser surface

TABLE 1
Pattern details and laser processing parameters for the CO_2 laser surface engineered PET.

	Track		Hatch	
Pattern	**CO2_4T**	**CO2_5T**	**CO2_4H**	**CO2_5H**
Centre-to-centre spacing (μm)	350	400	350	400
Power (W)	6	6	6	6
Traverse speed (mm/s)	400	400	400	400
Beam diameter (mm)	95	95	95	95
No. of samples	18	18	18	18

engineered patterns. These track samples were labelled CO2_4T and CO2_5T and the hatch samples were labelled CO2_4H and CO2_5H, for 350 and 400 μm spacings, respectively, for both patterns. It should be noted here that the dimensions stated for the laser engineered samples are those of the CO_2 laser scanning dimensions and not of the resulting laser engineered patterns. A total of 18 samples were produced for each of the four sample sets. Full details are given in Table 1.

2.1.3 KrF excimer laser surface engineering methodology

A KrF excimer laser (EMG 203 MSC; Lambda Physik, GmbH) emitting a raw 23×12 mm^2 beam at 248 nm was used to irradiate a large section of each billet at a time. In order to hold the sample normal to the beam, a bracket on the optical train was used.

Sample sets of two different track and two different hatch patterns were produced: tracks with 100 pulses at 100 mJ (EX_1T) and 100 pulses at 200 mJ (EX_2T), and hatch patterns with 100 pulses at 100 mJ (EX_1H) and 100 pulses at 200 mJ (EX_2H). This gave fluences of 36 and 72 mJ/cm^2, respectively for the different energies used. For both sample sets the repetition rate was kept constant at 25 Hz and an Aerotech computer numerical control (CNC) programming ensured that the correct number of pulses was applied to each sample. A spacing of 350 μm was used for both sample sets. It should be noted here that the dimensions stated for the laser engineered samples are those of the KrF laser scanning dimensions and not of the resulting laser engineered patterns. A total of 18 samples were produced for each of the two sample sets. Full details are given in Table 2.

2.2 Topographical and chemical analysis techniques

Before and after laser surface engineering the PET films were analysed using a scanning electron microscope (SEM) (TM3030 Plus; Hitachi Corporation) to determine the morphological and microstructural characteristics.

To ascertain phase characteristics of the as-received and laser engineered billets X-ray photoelectron spectroscopy (XPS) data was acquired. This was

TABLE 2
Pattern details and laser processing parameters for the KrF excimer laser surface engineered PET.

	Track		Hatch	
Pattern	**EX_1T**	**EX_2T**	**EX_1H**	**EX_2H**
Centre-to-centre spacing (μm)	350	350	350	350
Pulse width (ms)	30	30	30	30
No. of pulses	100	100	100	100
Energy (mJ)	100	200	100	200
Fluence (mJ/cm^2)	36	72	36	72
No. of samples	25	25	25	25

done using a bespoke ultra-high vacuum system fitted with a 150 mm mean radius hemispherical analyser with a 9-channeltron detection (Phoibos; Specs GmbH). XPS spectra were acquired using a non-monochromated Al Kα X-ray source at 1486.6 eV. Survey spectra were acquired over the binding energy range 1100 to 0 eV using a pass energy of 50 eV and high resolution scans were made over the C 1s and O 1s lines using a pass energy of 15 eV. In each case the analysis was an area average over a region approximately 2 mm in diameter on the sample surface. The energy scale of the instrument is calibrated according to ISO standard 15472, and the intensity scale is calibrated using an in-house method traceable to the UK National Physical Laboratory. Data were quantified using Scofield cross sections corrected for the energy dependencies of the electron attenuation lengths and the instrument transmission. Data interpretation was carried out using CasaXPS software v2.3.16.

The surface topography of the as-received and the laser engineered billets was analysed using a confocal chromatic imager (CCI) profilometer (Micromersure2, STIL SA.). Sample sizes of 0.5×0.5 mm^2 were examined for each of the billets analysed. Three CO_2 laser surface engineered, three KrF excimer laser surface engineered and three as-received control billets were analysed. The laser modified samples were ultrasonically cleaned in acetone, ethanol then de-ionized water (dH_2O) for three minutes each at room temperature before measurements were taken. The results were analysed using SurfaceMaps software (STIL SA.) and were expressed as R_a (the arithmetic mean of the departures of the roughness profile from the mean line) and S_a (the surface roughness calculated over an area). Data for R_t (maximum height of profile) and R_{sk} (skewness: symmetry of the profile about the mean) surface parameters were included in order to provide more information on the topographical features of the surfaces.

2.3 Wettability characteristics analysis methodology

Measurement of wettability characteristics is still fraught with complications; however, this study requires comparative data for untreated and laser treated

PET surfaces and so contact angle, θ, measurements were obtained using a goniometer (OCA100; DataPhysics Instruments, GmbH) using the needle-in advancing method, a method deemed and demonstrated previously [44-52] to be more than adequate. Two liquids were used: water and diiodomethane. Prior to contact angle measurements being taken the untreated and laser surface engineered billets were ultrasonically cleaned in acetone, ethanol and finally dH_2O for three minutes each at room temperature. The dH_2O step was included here to remove any residue left on the PET surface resulting from the acetone and ethanol cleaning stages. To ensure that the sample surfaces were dry, the billets were placed in a specimen dryer (SS; LEEC, Ltd.) for 30 minutes before contact angle measurements were taken.

The surface free energy, γ_s, of the as-received and laser surface engineered PET was ascertained through initial consideration of the contact angles and application of Young's equation:

$$\cos\theta = \frac{\gamma_s - \gamma_{sl}}{\gamma_l} \tag{1}$$

where γ_l is the surface tension of the liquid and γ_{sl} is the interfacial energy between the solid and the liquid and can be rewritten as

$$\gamma_s = \gamma_{sl} + \gamma_l \cos\theta \tag{2}$$

In order to calculate γ_s from the gathered value of θ, the second unknown variable, γ_{sl}, in Equation (2) must be determined. Fowkes [53] has proposed partitioning the surface free energy into individual components which assumes that interfacial interactions arising from the properties of the measuring liquid and surface layer determine the quantity γ_s, stating that the surface free energy of a solid is composed of a sum of individual components:

$$\gamma_s = \gamma_s^d + \gamma_s^p + \gamma_s^h + \gamma_s^i + \gamma_s^{ab} + \gamma_s^o \tag{3}$$

where γ_s^d, γ_s^p, γ_s^h, γ_s^i and γ_s^{ab} are the dispersive (London), polar, hydrogen, induction and acid-base components, respectively, with γ_o^s denoting all other interactions that may be present in the system. The Owens, Wendt, Rabel and Kaelble (OWRK) method [54] furthered the work of Fowkes by assuming that all the components on the right-hand side of Equation (3), apart from γ_s^d, can be associated with and therefore incorporated in γ_s^p. These similar interactions between the phases are interpreted as the geometric mean of the dispersive and polar parts, leading to

$$\gamma_{sl} = \gamma_l + \gamma_s - 2\left(\sqrt{\gamma_l^d \gamma_s^d} + \sqrt{\gamma_l^p \gamma_s^p}\right) \tag{4}$$

where γ_s^p and γ_l^p are the polar components, and γ_s^d and γ_l^d are the dispersive components of the solid and liquid, respectively. If Equation (4) is substituted into Equation (2) then we have

$$y_s = \gamma_l + \gamma_s - 2\left(\sqrt{\gamma_l^d \gamma_s^d} + \sqrt{\gamma_l^p \gamma_s^p}\right) + \gamma_l \cos\theta \tag{5}$$

and rearranging yields

$$\gamma_l(1 + \cos\theta) = 2\left(\sqrt{\gamma_l^d \gamma_s^d} + \sqrt{\gamma_l^p \gamma_s^p}\right) \tag{6}$$

Equation (6) brings forth two unknown variables: γ_s^d and γ_l^p. If Equation (6) is now transposed in the form of a general equation for a straight line:

$$\frac{\gamma_l(1 + \cos\theta)}{2\sqrt{\gamma_l^d}} = \sqrt{\gamma_s^p}\sqrt{\frac{\gamma_l^p}{\gamma_l^d}} + \sqrt{\gamma_s^d} \tag{7}$$

then γ_s^d is found from the axis intercept point and γ_l^p is found from the slope of the linear graph produced using water, ethylene glycol and diiodomethane test liquids. We can now insert the values of γ_s^p and γ_s^d into Equation (4) to determine the value of γ_{sl}. Thereafter, the value of γ_{sl} is inserted into Equation (2) with the appropriate values for γ_l and θ to calculate the value of γ_s. The associated software used by the goniometer employed in this work use the OWRK method to automatically calculate the value of γ_s.

2.4 Statistical methods

Statistical analysis was performed by two-way analysis of variance combined with Tukey's Post Hoc analysis with $p \geq 0.05$ considered significant. All data has been analysed using SPSS statistics 22.0 (IBM) and graphical representation of results were produced using SigmaPlot 13.0 (Systat Software, Inc.).

3 RESULTS AND DISCUSSION

3.1 Topographical analysis

The patterns of the PET film surfaces engineered by the CO_2 laser beam interaction depend upon both the optical system parameters and the material properties of the polymer .[31, 51, 55]. The laser parameters determine the incident laser power, spot size, depth of field and divergence of the laser beam, while the thermophysical properties of the polymer determine how the polymer reacts to the beam. The resulting profile seen in Figure 1 of the CO_2

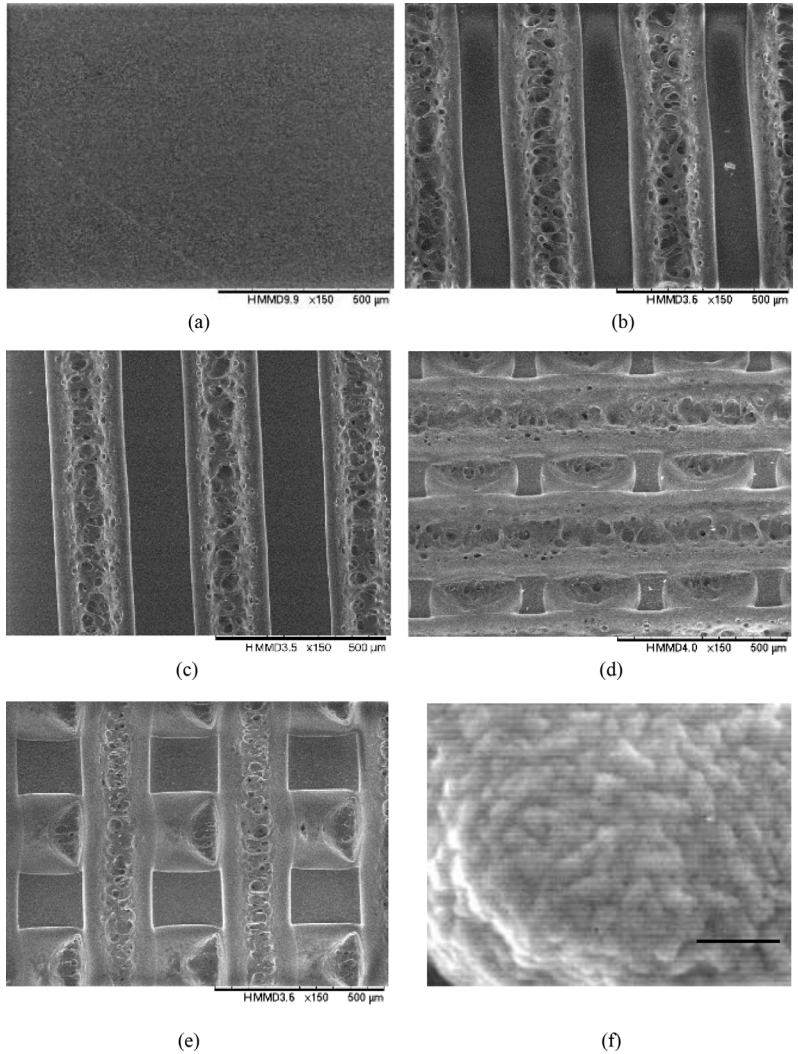

FIGURE 1
SEM micrographs of (a) as-received (AR) PET sample and CO_2 laser surface engineered PET films: (b) CO2_4T; (c) CO2_5T; (d) CO2_4H; (e) CO2_5H; and (f) a KrF excimer laser surface engineered film (EX_1T).

laser engineered patterns and the heat affected zone (HAZ) are a result of the combination of these factors.

From the SEM micrographs shown in Figures 1(b) to (e) it can be seen that as a direct result of the interaction of the CO_2 laser beam with the PET film surfaces, features were created *via* controlled and selective melting. This

is evidenced by the craters formed from bubbles and subsequent resolidification which has formed the different track patterns shown in Figures 1(a) to (j). This complicated structure is likely associated with the thermally induced stress release in the biaxially oriented film caused by the CO_2laser beam interaction with the PET film [56]. In comparison to the track patterns (*cf.* Figures 1(b) to (f)), both hatch patterns (*cf.* Figures 1(h) to (j)) have resulted in wider tracks being formed along the ordinate direction of the pattern. This is because the CO_2 laser beam actually processes the PET surface twice, with the CO_2 laser beam passing over the initial track to create the hatch, causing the PET surface to remelting and resolidify, naturally creating larger surface features. The remelting and resolidification of the material on the hatch pattern has also resulted in some of the patterning becoming changed. Where the CO_2 laser beam has passed over the underlying track, the sides have been remelted and part of the track has subsequently filled in. Even so, the overall hatch and track patterns appear clean and well structured. It is worth noting that no discernible HAZ was observed under optical microscopic analysis (see Figures 1(a), (c), (e), (g) and (i)) and, therefore, the areas between the tracks were considered as as-received material.

The surface morphology of the PET changed little after KrF excimer laser surface engineering, so only SEM micrographs were used to examine the surface. A typical SEM micrograph for KrF excimer laser surface engineered sample EX_1T is shown in Figure 1(k), which shows the morphology to be formed of sphere-like aggregates.

The surface roughness values of the laser treated PET samples varied in accordance with the laser used. The value of the R_a parameter was found to have increased considerably, from 0.06 $\pm$0.01 μm for the as-received control sample (AR) up to 8.58 $\pm$0.91 μm for CO2_4T and 6.22 $\pm$ 0.79 μm for CO2_5T (see Table 3). Similarly, the value of the S_a surface roughness parameter experienced a marked increase from 0.22 $\pm$0.13 μm for AR up to 22.80 $\pm$4.43 μm for CO2_4T and 10.47 $\pm$0.12 μm for CO2_5T. The increase in surface roughness between AR and both CO2_4T and CO2_5T was found to be statistically significant with a mean difference of 8.58 μm, $p < 0.01$ and 6.62 μm, $p < 0.01$ for R_a, respectively; and 22.58 μm, $p < 0.01$ and 10.24 μm, p=0.01 for S_a, respectively. Table 3 shows that both the R_a and S_a surface parameters for samples CO2_4H and CO2_5H were found to have increased markedly compared to AR. This discernible increase in surface roughness between the as-received sample and both hatch patterned samples was found to be statistically significant, with $p < 0.05$. From Table 3 one can see that along with an overall increase in surface roughness, R_a and S_a for samples CO2_4T and CO2_4H increased more in comparison with the wider spaced track and hatch patterned samples CO2_5T and CO2_5T. This difference in R_a and S_a increase was statistically significance with $p < 0.05$ and

TABLE 3
Surface parameter data for each sample.

Sample	R_a (μm)	S_a (μm)	R_t (μm)	R_{sk}
AR	0.06 ±0.01	0.22 ±0.13	0.36 ±0.04	−0.09±0.24
CO2_4T	8.58 ±0.91	22.8 ±4.43	49.03 ±8.43	0.45 ±0.41
CO2_5T	6.22 ±0.79	10.47 ±0.12	43.50 ±5.05	0.06 ±0.26
CO2_4H	16.13 ±1.33	35.23 ±3.12	107 ±2.65	−1.21±0.47
CO2_5H	13.07 ±0.81	22.8 ±0.92	116 ±4.36	−0.98±0.77
EX_1T	0.19 ±0.11	3.70 ±0.15	0.48 ±0.08	0.05 ±0.15
EX_2T	0.23 ±0.19	3.88 ±0.18	0.56 ±0.08	0.09 ±0.12
EX_1H	0.20 ±0.36	3.56 ±0.08	0.46 ±0.10	0.08 ±0.18
EX_2H	0.21 ±0.35	3.64 ±0.08	0.46 ±0.12	0.08 ±0.07

is due to CO_2 laser beam processing of a larger surface area of the CO2_4T and CO2_4H samples which, in turn, created a markedly rougher surface. The statistical significances between the as-received PET film and the CO_2 laser engineered film is unsurprising as the CO_2 laser modification produced well defined topographical features, as is apparent from the change in R_t (total height of the profile). Both hatch patterns achieved the peak/valley distances measuring 107.00 ±2.70 μm for CO2_4H and 116.00 ±4.40 μm for CO2_5H, compare to the peak/valley distances of the single track patterned samples or the as-received sample. As discussed above, this difference is explained by the second pass of the CO_2 laser beam over the PET sample surface on the hatch pattern billets, which was 90^o to the first pass resulting in double the amount of CO_2 laser beam-material surface interaction where the two tracks passed. This can also be seen in the optical and SEM images given in Figure 1.

In contrast, Table 3 shows that the R_a parameter for the KrF excimer laser treated PET samples EX_1T and EX_2T increased only marginally in comparison to 0.19 ±0.11 μm and 0.23 ±0.19 μm, respectively; nevertheless, this still represents an order of magnitude increase. The same was true for the value of the S_a surface roughness parameter, increasing to 3.70 ±0.15 μm and 3.88 ±0.18 μm for EX_1T and EX_2T, respectively. The increase in surface roughness between AR and both EX_1T and EX_2T was found to be statistically significant with a mean difference of 0.19 μm, ($p = 0.01$) and 0.23 μm, ($p = 0.01$) for R_a, respectively; and 3.70 μm, ($p < 0.01$) and 3.88 μm, ($p = 0.01$) for S_a, respectively.

3.2 Surface chemistry analysis

3.2.1 Composition and functional groups

XPS results are given in Table 4 and shown in terms of at.% and are normalised to 100% excluding H and He, which are not detected by the

TABLE 4
Surface compositions of the as-received and laser surface engineered PET samples as determined by XPS.

Element and Photoelectron Line	**Surface Composition (at.%) for Each Sample**								
	AR	**CO2_4T**	**CO2_5T**	**CO2_4H**	**CO2_5H**	**EX_1T**	**EX_2T**	**EX_1H**	**EX_2H**
Na 1s	0.3					0.1	0.1	0.1	0.1
O 1s	24.6	25.6	25.2	26.0	26.1	34.5	36.8	34.3	37.8
N 1s	2.2	0.7	0.4	1.1	0.6	1.8	2.2	2.0	2.1
Ca 2p	0.3								
C 1s	71.7	72.5	73.0	71.7	72.6	72.4	75.7	73.3	74.1
S 2p	0.2								
P 2p	0.1								
Mg 2s	0.7	0.2	0.3	0.4	0.4	0.7	0.6	0.7	0.6
Si 2s/2p	0.03		0.10	0.70	0.20	0.19	0.24	0.21	0.29
F 1s					0.2				

technique. In all cases, the data show C and O_2 in approximately the corrected atomic ratio expected for a pure PET reference sample, along with a number of lower level species. The lower level species include N, Ca, Na, S, P, Si and F. These are typical surface contamination elements resulting from handling and general exposure to the laboratory environment, and the amounts detected indicate sub-monolayer levels on the outer surface of the samples. One can see from Table 4 that the overall level of these surface contaminant species was reduced by the CO_2 laser surface engineering – likely the result of low levels of local surface vaporization. The story was similar for the KrF excimer laser surface engineering, but in this instance the reduction in surface contaminant species would have resulted from the ultraviolet (UV) light ablation of the upper surface layers of the PET that contained the contaminants.

When viewing the results of Table 4 it is unsurprising that the spectra from the as-received and CO_2 laser engineered were seen to be similar. The survey spectrum and the higher resolution scans over the C 1s and O 1s lines from the CO_2 laser engineered CO2_SP04 sample are shown in Figure 2(a) as typical for example purposes. Apart from the presence of the minor surface contaminant species, the spectra are in very good agreement with reference data from pure spin-cast PET [57]. In Figure 2(b) and Figure 2(c) the C 1s and O 1s spectra have been deconvoluted to permit closer inspection of the surface functional groups. The C 1s spectrum shows components due to C-C bonds, C in ether bonds and C in ester bonds. The O 1s spectrum shows components due to oxygen in ether and carbonyl/ester groups, as expected. There was no significant modification of the number or relative proportions of

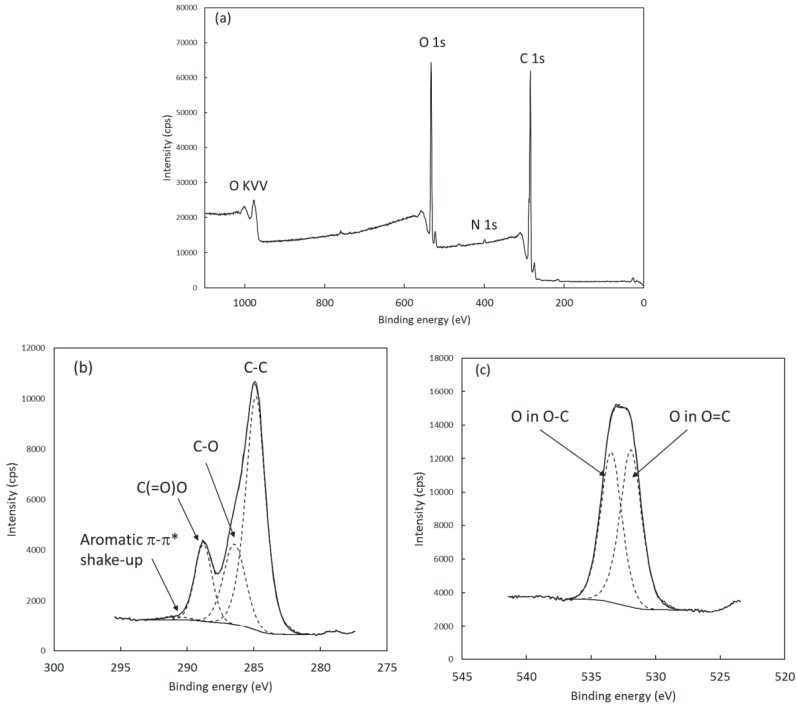

FIGURE 2
XPS spectra from the surface of CO2_4T showing (a) survey spectrum with principal peaks labelled (the small peak at around 760 eV binding energy is an artefact and should be ignored), and (b) and (c) higher resolution deconvoluted C 1s and O 1s spectra with chemically-shifted components labelled.

these components through the entire series of CO_2 laser engineered samples, both in reference to one another (including the as-received sample (AR)) and the reference PET data. Small differences in the levels of trace contaminants aside, the spectra given in Figure 2 reveal there to be very little change in the surface chemistry of the PET after CO_2 laser treatment.

Such negligible changes in the surface chemistry of polymers after interaction with infrared (IR) laser beams have been reported before. Lawrence and Li [49, 50] and Waugh and Lawrence [52] found that when surface treating polymethyl methacrylate (PMMA) and polyethylene (PE) with CO_2, Nd:YAG and high power diode laser (HPDL) beams, very little change in surface chemistry of the polymers could be discerned. As Figures 1(b) to (e) show, the melting induced on the surface of the PET with CO_2 laser irradiation is selective and controlled with respect to area and time in the molten state. Previous work demonstrates that temperature influences oxygen uptake

by polymers. Hawkins *et al.* [58] showed many years ago that oxidation of polymers in the solid state was substantially less than in the molten state and Marechal *et al.* [59] revealed that the extent of time in the molten state correlated to more oxidation. Waugh [45, 51] CO_2 laser surface engineered nylon 6,6 in a whole area manner, resulting in a high level of melting for a sufficiently long period of time to bring about significant oxygen diffusion.; indeed, Table 4 suggests that the CO_2 laser processing parameters employed here brought about a level of melting insufficient to trigger oxygen absorption adequate to start effecting contact angle. In contrast with this work we have controlled melting at low power and high speed, resulting in little to no oxygen diffusion;

The findings of Lawrence and Li [49, 50], however, revealed that the effects of laser-induced surface chemistry changes cannot be completely discounted, especially surface oxygen content. These workers discovered laser beam wavelength range to be a factor in triggering surface chemistry changes in polymers, categorizing IR laser beams as bringing about little to no change, whilst UV laser beams precipitated significant changes.

As one can see from Table 4, after interaction with the KrF excimer laser beam the surface oxygen content of the PET increased markedly. An increase in surface oxygen content of a number of polymer materials after excimer laser interaction has been documented [49, 50, 60]. Such an occurrence is due to the fact that polymers undergo main-chain scission when subjected to concentrated levels of UV radiation in air [61], increasing the C-O bonds (esters and alcoholic groups) and O=C-O bonds (esters carboxyl groups) [62]. The C-C bonding was seen to decrease. This is explained by the photon energy of the KrF laser beam of 643.8 kJ/mol being sufficient to induce chain scission of the C-C bonds, which have a bonding energy of 347 kJ/mol. In addition, oxidative decomposition and volatization by the excited oxygen atoms $O(^1D)$ will have taken place and created oxygen functionalities of the C-O and O=C-O bonds on the PET surface [61]. So, when exposed to the excimer laser radiation under the selected laser operating parameters, the PET can easily generate free radicals as transient species. The oxygen in the air can then readily react with the free radicals under the high temperatures generated on the surface of the PET. It is suggested that oxidation in this manner is the reason for the observed increase in the surface oxygen content of the PET after KrF excimer laser treatment.

3.2.2 Crystallinity

The complexity of the vibrational spectrum of partially crystalline PET is a result of the split of the absorption bands into amorphous and crystalline modes and also the fact that they are sensitive to chain configuration and orientation [63]. Due to this, assignment of the bands to crystalline and amorous

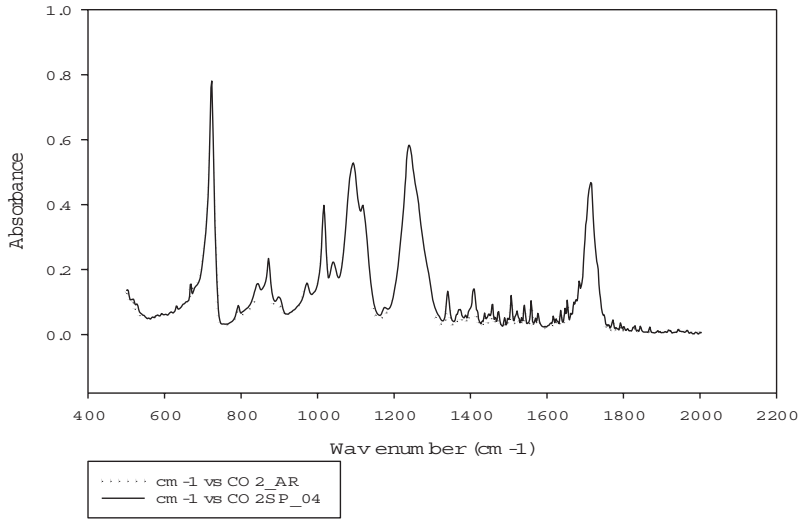

FIGURE 3
ATR-FTIR spectrum of the as-received material (AR) in comparison with a CO_2engineered PET film with track spacing of 350 μm (CO2_4T).

regions has proven to be difficult and led to ongoing differences in interpretation; however Chen *et al.* [63] found the carbonyl absorption band has a maximum absorption in the amorphous regions at 1727 cm^{-1} and at 1717 cm^{-1} in crystalline material, such that on crystallization the intensity of the higher wavenumber band decreases and is progressively shifted to lower wavenumber. These changes make the ratio of the two carbonyl absorption bands a convenient method of measuring the fractional crystallinity of PET.

Figure 3 gives the ATR-FTIR spectra of the as-received (AR) and a CO_2 laser modified (CO2_4T) PET sample (as typical for example purposes), both contrasted with the spectrum of PET from a standardized database (KnowItAll Informatics System 2014, BioRAD Laboratories). With reference to the as-received PET spectra, the band at 1717 cm^{-1} has increased for CO2_4T, suggesting that the CO_2 laser surface engineering resulted in higher crystallinity. In contrast, ATR-FTIR spectra for the KrF excimer laser modified PET showed no discernible difference to that of the as-received spectra. This is not surprising because the KrF laser beam-PET interaction at the fluences used effected atomic layer-scale ablation only, not being sufficiently high to result in any reordering or melting. The work of Hsu *et al.* [64] revealed that KrF laser fluences of greater than 2 J/cm^2 were needed to bring about changes to the crystallinity of PET.

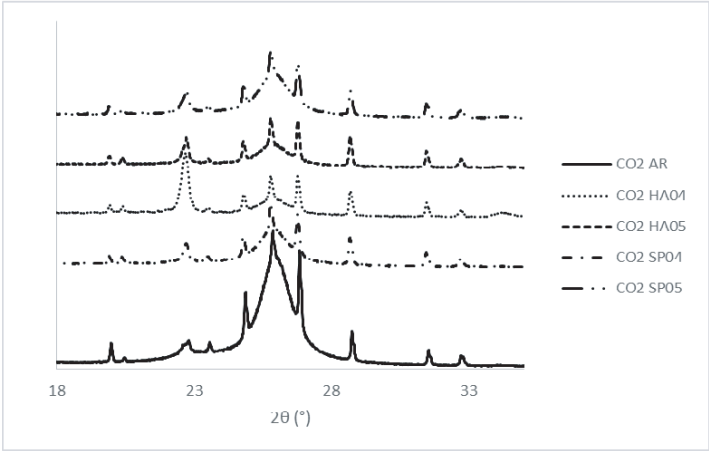

FIGURE 4
XRD plot of PET films before (AR) and after CO_2 laser surface engineering.

The XRD patterns with 2θ between 18.0 and 35.0° of the as-received and CO_2 laser engineered PET films are given in Figure 4. After CO_2 laser treatment the peak at 26.0° sharpens and shifts slightly to the left (25.8°) while a peak at 34.2° begins to appear, also suggesting the crystallinity of the PET films has increased after the patterns were engineered on to the surface using the CO_2 laser beam. It is reasonable to say that the CO_2 laser-induced resolidification process favours a more crystalline structure, implying that the laser process is effectively reducing the level of entanglement within the polymer allowing a somewhat more ordered structure to be established. This is possibly due to the short, but intense melt applied by the CO_2 laser beam as a result of such IR wavelengths acting as heat sources. The abrupt, and directional, removal of the heat source caused by inherent the rapid processing associated with lasers is likely what facilitates this ordering of the polymer. The fact that there was no such melting and resolidification process taking place during KrF excimer laser surface engineering of the PET samples means that there would be no occurrence of peak shifting to be observed from XRD analysis, indicating that there was no real change in the crystalline nature of the material.

3.3 Wettability performance and the hydrophilic/hydrophobic reaction

Table 5 shows that CO_2 laser engineering of the PET surface brought about an across the board statistically significant ($p < 0.05$) increase in contact angle. The measured contact angles were, for the most part, doubled from the

TABLE 5
Contact angle formed by water droplets on the PET samples and the corresponding surface energy values.

Sample	Contact Angle, $\theta(^o)$	Surface Free Energy, γ_s (mJ/m^2)	Polar Component, γ^p (mJ/m^2)
AR	77.7 ±2.2	36.5 ±0.4	29.6 ±0.5
CO2_4T	137.1 ±2.3	4.3 ±2.3	2.3 ±2.4
CO2_5T	143.2 ±2.9	2.5 ±0.7	1.7 ±0.7
CO2_4H	114.2 ±4.4	15.3 ±0.9	8.0 ±0.88
CO2_5H	116.2 ±5.5	17.6 ±5.6	9.7 ±3.2
EX_1T	34.5 ±2.4	60.2 ±3.4	36.5 ±0.1
EX_2T	35.1 ±2.5	62.4 ±3.2	37.1 ±0.1
EX_1H	30.5 ±2.2	77.3 ±3.5	42.3 ±0.1
EX_2H	28.5 ±2.3	80.7 ±3.2	43.8 ±0.2

hydrophilic as-received sample, with all CO_2 laser engineered PET contact angles being hydrophobic and greater than 100^o. In contrast, the measured contact angles for the KrF excimer laser engineered PET surfaces experienced increased hydrophilicity, with the contact angle for all samples reducing statistically significantly ($p < 0.04$) by at least half from the as-received sample.

Laser surface engineering produced marked changes in the surface free energy and the polar component of the surface free energy of the PET, as can be seen from Table 3. When subjected to CO_2 laser surface engineering surface free energy of the PET fell by a statistically significant ($p < 0.01$) order of magnitude, as too did the polar component of the surface free energy of the PET ($p < 0.01$). The opposite effect took place on the PET surfaces following KrF excimer laser treatment. Here it can be seen from Table 5 that considerable increases in surface free energy ($p = 0.01$) and polar component of the surface free energy of the PET ($p < 0.01$) occurred.

It is possible now to consider the laser-induced changes in the PET wettability characteristics with reference to the gathered topographical and chemical data. CO_2 laser surface engineering induced a change in the wettability characteristics of the PET from the hydrophilic as-received state to post-CO_2 laser processed hydrophobic state. Table 4 and Figure 2 show statistically negligible change in the surface chemistry of the CO_2 laser engineered PET, whilst Figure 3 and Figure 4 shows some marginal increased crystallinity; however, Table 3 shows statistically significant changes in topography, with every measure of roughness and surface asperity increasing many fold. In terms of topography the same was observed for the KrF excimer laser engineered PET surfaces, although, still statistically significant, the magnitude of change was less pronounced when compared with the effects of CO_2 laser radiation. But, Table 4 reveals statistically significant changes in the surface

chemistry of the KrF excimer laser engineered PET, particularly in the O 1s line which denotes an increase in the surface oxygen content. All of this has culminated in the PET surface becoming more hydrophilic as a result of KrF excimer laser surface engineering.

Wetting is known to be governed by the first atomic layers of the surface of a material and the oxygen content of a material's surface is an influential factor governing its wetting performance [66, 67]. In an untreated state peaks in the O 1s spectrum of PET are assigned to O=C (esters) bonding (O1) and O-C (ethers) bonding (O2). Table 4 shows that the O 1s spectra of the KrF excimer laser surface engineered PET samples showed a statistically significant increase in O=C esters and carboxyl groups, and O-C bonding of ethers and carboxyl groups. Naturally then, polar components such as alcoholic and carboxyl groups would form on the KrF excimer laser engineered PET surfaces. This indicates that there is agreement between the XPS spectra results in Table 4 and the calculated surface free energy values given in Table 5. In addition, these results show that the KrF excimer laser surface engineering multiplied the hydrophobicity of the PET surface through the creation of additional polar components, as clearly demonstrated by the results given in Table 5. Interestingly, the increased crystallinity of the PET surface that can be seen in Figure 3 and Figure 4 resulting from CO_2 laser interaction appears to have not influenced the wettability characteristics. Table 4 shows there to be no significant change in the O 1s spectrum of the CO_2 laser engineered PET surfaces, whilst Table 5 shows that a considerable reduction in surface free energy and polar component of the surface free energy of the PET took place. Clearly, the reduction in polar component indicates that oxygen-containing polar functional groups were not generated because the IR nature of the CO_2 laser beam operated with the chosen parameters did not cause photo-oxidation on the PET surface. Again, this result is in agreement with the XPS data in Table 4 and the calculated surface free energy values given in Table 5.

At this point it can be asserted from the findings that the observed increase from the as-received condition in contact angle undergone by all CO_2 laser engineered PET was driven by the changes in surface topography. Wetting of a rough surface can either follow the Wenzel, Cassie-Baxter or an intermediate mixed-state regime [65], as shown in Figure 5.

In a homogeneous wetting situation described by Figure 5(a), then Wenzel's equation stands as providing an approximation of the contact angle:

$$\cos\theta = \frac{r_a(\gamma_s - \gamma_{sl})}{\gamma_{lv}} \tag{8}$$

where r_a is the roughness factor defined as the ratio of the real and apparent surface areas. In this instance, unless extremely large changes are made

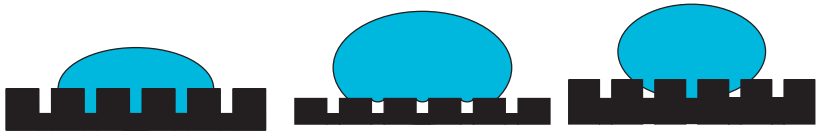

FIGURE 5
Schematic diagram showing a droplet of water on a patterned surface giving rise to (a) the Wenzel wetting regime, (b) the Cassie-Baxter wetting regime and (c) an intermediate mixed-state wetting regime.

to the surface chemistry of the material, large enough to increase greatly the polar component of the surface free energy of the PET, then the surface roughness will effectively solely govern changes to the contact angle. So, essentially one can see that for the CO_2 laser engineered PET surfaces with their much rougher surfaces and effectively unchanged surface oxygen content, and thus the almost unchanged polar component of the surface free energy of the PET, would inherently follow the theoretical framework given by Wenzel's equation and lead to an increased contact angle in accordance with Equation (8). In a heterogeneous wetting situation described by Figure 5(b), then the Cassie-Baxter equation stands as providing an approximation of the contact angle:

$$\cos\theta = \frac{r_a f(\gamma_s - \gamma_{sl})}{\gamma_{lv}} + f - 1 \tag{9}$$

where f is the fraction of the solid surface area wet by the liquid. Again, one can see from the Cassie-Baxter equation that without sufficiently large increases in the polar component, then the surface roughness will be the singular factor at play to determine changes to the contact angle. So once again, because the CO_2 laser engineered PET surfaces are dominated by their rougher surfaces and almost unchanged polar component of the surface free energy, they will certainly follow the theoretical framework given by Cassie-Baxter equation, causing contact angle increases in accordance with Equation (9). At present there is no accepted mathematical expression for intermediate mixed-state wetting regime; nevertheless, it is still reasonable to state that regardless of the type of rough surface, surface roughness dominates contact angle values on the CO_2 laser engineered PET surfaces simply because of the virtual absence of the necessary chemical changes required to increase the polar component of the surface free energy value. There is a very different regime at play governing the contact angle of the KrF excimer laser surface engineered PET. Here the contact angle has decreased despite the KrF excimer laser irradiation roughening the PET surface. This surface

TABLE 6
Selected surface parameter data, selected surface compositions, and contact angle formed by water droplets and the corresponding surface energy values for CO_2 and KrF excimer laser surface engineered PET samples in ambient air and oxygen-rich atmospheres.

Sample	R_a (μm)	S_a (μm)	O 1s (at.%)	C 1s (at.%)	Contact Angle, $\theta(^o)$	Surface Free Energy, γ_s (mJ/m^2)	Polar Component, γ^p (mJ/m^2)
CO2_4T	8.58 ±0.91	22.8 ±4.43	26.6	72.5	137.4 ±2.3	4.25 ±2.29	2.27 ±2.42
CO2_4T_O	8.61 ±0.89	23.4 ±4.34	29.7	72.6	121.3 ±1.8	6.87 ±2.08	3.89 ±1.70
EX_2T	0.23 ±0.19	3.88 ±0.18	36.8	72.7	35.1 ±2.5	62.36 ±3.24	37.12 ±0.12
EX_2T_O	0.20 ±0.21	3.79 ±0.15	39.4	73.2	28.4 ±1.2	68.41 ±2.05	39.98 ±0.42

roughening, according to Equation (8) and Equation (9), should have brought about an increase in the contact angle - the reverse of what was actually observed. Clearly, the chemical changes in the shape of enhancement of the oxygen-rich functional groups and the subsequent increased polar nature of the surface of the PET after KrF excimer laser irradiation have influenced the contact angle value; indeed, as a number of workers have seen [64, 65, 46-48], when polymers have an increased polar nature to their surfaces this overrides, to a degree, the effect on contact angle of increased surface roughness. Even though the increase in surface roughness of KrF excimer laser engineered PET was not as much as that of the CO_2 laser surface engineered samples, it was still an order of magnitude increase over the as-received sample that ought to have yielded an increase in contact angle according to Equation (8) and Equation (9). Considering this aspect further reinforces the counteractive influence that the increased polar nature of the PET surface has on the contact angle.

To explore this PET surface roughness- polar component of the surface free energy of the PET finding further, additional work was carried out. This involved reprocessing a PET sample with the CO_2 laser and KrF excimer laser beams using selected previous experimental parameters. The sample sets selected were CO2_4T and EX_2T, but in this new experimental work they were laser surface engineered within an oxygen-rich atmosphere rather than in ambient air. This new sample set was CO2_4T_O for the CO_2 laser and EX_2T_O for the KrF excimer laser.

It is clear from Table 6 that laser processing in the presence of an increased oxygen atmosphere, regardless of the laser source, influences contact angle. With surface topography remaining the same as the samples processed in ambient air, this atmosphere richer in oxygen has resulted in the laser engineered PET surfaces becoming more polar which, in turn, has brought about a reduction in contact angle. The CO_2 laser surface engineered sample processed in the oxygen-rich atmosphere (CO2_4T_O) is still

hydrophobic, but Table 4 shows that surface oxygen increased and contact angle decreased from the equivalent sample treated in air (CO2_4T). The effect of the oxygen-rich atmosphere on the KrF excimer laser surface engineered sample (EX_2T_O) was the make its surface even more polar in nature and this caused the contact angle to decrease from the equivalent sample treated in air (EX_2T).

4 CONCLUSIONS

Using laser beam wavelength and selected operating parameters as a means for the controlled surface engineering of polyethylene terephthalate (PET) to deliver tailored surfaces with bespoke levels of wettability has been demonstrated. The science and technology underpinning this work will be applicable to most polymers. The key findings resulting from this work are:

(i) CO_2 laser surface engineering is capable of generating surface features without modifying the chemical composition of the PET surface layer;

(ii) As well as being capable of generating surface features, KrF excimer laser surface engineering also modifies chemistry of the PET surface layer;

(iii) Since CO_2 laser surface engineering of the PET effects no chemistry change, then no change in the polar nature of the PET surface occurs. The topography is rougher in nature after CO_2 laser surface engineering so contact angle follows the theories of Wenzel, *etc*. and increases. This caused the surface of the PET to change from hydrophilic to hydrophobic;

(iv) KrF excimer laser surface engineering changed both the topography and chemistry of the surface of the PET, resulting in a surface that was rougher and more oxygen-rich with functional groups enhanced to make surface more polar in nature. This increased polar characteristic has more of an effect than the topography so contact angle decreased and the surface of the PET became more hydrophilic; and

(v) The governing effect of surface oxygen content on the polar component of the surface free energy of the PET was verified when conditions were set (processing in an oxygen-rich atmosphere) to bring about an increase on surface oxygen content in the PET surface. After both CO_2 and KrF laser surface engineering under such conditions, the contact angle decreased in both cases despite no change in topography.

This work contributes to the wider knowledge base around the laser surface engineering of polymers, moving it towards a new science-based

platform from where it is possible to design and fabricate at scale wettability characteristics that render the polymer suitable for a given application. The outcome of being able to manipulate the polar component of the surface free energy of the PET (through atmospheric oxygen content) and control the contact angle behaviour of the surface of PET presents new opportunities in many areas. Such opportunities include a controllable means for designing and producing anti-bacterial barriers at scale on polymer sheets and films, and improved adhesion and peel characteristics on polymer films used in packaging.

ACKNOWLEDGEMENTS

The authors are grateful to Sealed Air s.r.l. and Ishida Europe Ltd. for supplying the sample materials and financial support needed to complete this work.

REFERENCES

[1] Pietrikova A., Lukacs P., Jakubeczyova D., Ballokova B., Potencki J., Tomaszewski G., Pekarek J., Prikrylova K. and Fides M. Surface analysis of polymeric substrates used for inkjet printing technology. *Circuit World* **42** (2016), 9-16.

[2] Pedrow P.D., Sharmin S. and Freepons S.R. Plasma-modified interlayers applied to processing of polymer electronic materials, *The 33*rd *IEEE International Conference on Plasma Science*, Traverse City, Michigan, 2006 (IEEE, New York).

[3] Fahlman M. and Salaneck W.R. Surfaces and interfaces in polymer-based electronics. *Surface Science* **500** (2002), 904–922.

[4] Ozdemir M., Yurteri C.U. and Sadikoglu H. Physical polymer surface modification methods and applications in food packaging polymers. *Critical Reviews in Food Science and Nutrition* **39** (1999), 457–77.

[5] Appendini P. and Hotchkiss J.H. Review of antimicrobial food packaging. *Innovative Food Science and Emerging Technologies* **3** (2002), 113–126.

[6] Kim M.S., Khang G. and Lee H.B. Gradient polymer surfaces for biomedical applications. *Progress in Polymer Science* **33** (2008), 138–164.

[7] Pfleging W., Bruns M., Welle A. and Wilson S. Laser-assisted modification of polystyrene surfaces for cell culture applications. *Applied Surface Science* **253** (2007), 9177–9184.

[8] The K.S. and Lu Y.W. Topography and wettability control in biocompatible polymer for BioMEMs applications. *The 3rd IEEE Int. Conf. on Nano/Micro Engineered and Molecular Systems*, Sanya, China (2008), 1100–1103.

[9] Huang J., Murata H., Koepsel R.R., Russell A.J. and Matyjaszewski K. Antibacterial polypropylene *via* surface-initiation atom transfer radical polymerization. *Biomacramolecules* **8** (2007), 1396–1399.

[10] Hasan J., Crawford R.J. and Ivanova E.P. Antibacterial surfaces: The quest for a new generation of biomaterials. *Trends in Biotechnology* **31** (2013), 295–304.

[11] Zhao Q., Wang C., Liu Y. and T. Wang, Bacterial adhesion on the metal-polymer composite coatings. *International Journal of Adhesion and Adhesives* **27** (2007), 85–91.

[12] Harnett E.M., Alderman J. and Wood T., The surface energy of various biomaterials coated with adhesion molecules used in cell culture. *Colloids and Surfaces B* **55** (2007), 90–97.

[13] Jung Y.C. and Bhushan B. Contact angle, adhesion and friction properties of micro- and nanopatterned polymers for superhydrophobicity. *Nanotechnology* **17** (2006), 4970–4980.

[14] Ouhlal M., Xu R. and Schreiber H.P. Adhesion enhancement through control of acid-base interactions. *Journal of Adhesion* **80** (2004), 467–480.

[15] Speranza G., Gottardi G., Pederzolli C., Lunelli L., Canteri R., Pasquardini L., Carli E., Lui A., Maniglio D., Brugnara M. and Anderle M. Role of chemical interactions in bacterial adhesion to polymer surfaces. *Biomaterials* **25** (2004), 2029–2037.

[16] Milde F., Goedicke K. and Fahland M. Adhesion behaviour of PVD coatings on ECR plasma and ion beam treated polymer films. *Thin Solid Films* **279** (1996), 169–173.

[17] Zhao Q., Wang C., Liu Y. and Wang S. Bacterial adhesion on the metal-polymer composite coatings. *International Journal of Adhesion and Adhesives* **27** (2007), 85–91.

[18] Jung Y.C. and Bhushan B. Wetting transition of water droplets on superhydrophobic patterned surfaces. *Scripta Materialia* **57** (2007), 1057–1060.

[19] Waugh D.G., Lawrence J., Walton C.D. and Zakaria R.B. On the effects of using CO_2 and F_2 lasers to modify the wettability of a polymeric biomaterial. *Journal of Optics and Laser Technology* **42** (2009), 347–356.

[20] Liu G.J., Miyaji F., Kokubo T., Takadama H., Nakamura T. and Murakami A. Apatite-organic polymer composites prepared by a biomimetic process: Improvement in adhesion of the apatite layer to the substrate by ultraviolet radiation. *Journal of Materials Science: Materials in Medicine* **9** (1998), 285–290.

[21] Dadsetan M., Mirzadeh H., Sharifi-Sanjani N. and Daliri M. Cell behaviour on laser surface-modified polyethylene terephthalate *in vitro*. *Journal of Biomedical Materials Research* **57** (2001), 183–189.

[22] Ball M.D., Sherlock R. and Glynn T., Cell interactions with laser-modified polymer surfaces. *Journal of Materials Science: Materials in Medicine* **15** (2004), 447–449.

[23] Waugh D.G., Lawrence J., Morgan D.J. and Thomas C.L. Interaction of CO_2 laser-modified nylon with osteoblast cells in relation to wettability. *Materials Science and Engineering C* **29** (2009), 2514–2524.

[24] Waugh D.G. and Lawrence J. The enhancement of biomimetic apatite coatings by means of KrF excimer laser surface treatment of nylon 6,6. *Lasers in Engineering* **21** (2001), 95–114.

[25] Fourche G. An overview of the basic aspects of polymer adhesion. Part 2: Application to surface treatments. *Polymer Engineering and Science* **35** (1995), 968–976.

[26] Ladizesky N.H. and Ward I.M., A study of the adhesion of drawn polyethylene polymeric resin systems. *Journal of Material Science* **18** (1983), 533–545.

[27] Postema A.R., Doornkamp A.T., Meijr J.G., Vlekkert H.V.D. and Pennings A.J. Effect of chlorosulfonation of ultra high strength polyethylene fibres on mechanical properties and bonding with gypsum plaster. *Polymer Bulletin* **16** (1986), 167–171.

[28] Kaplan S.L., Rose P.W., Nguyen N.X. and Chang H.W. Corona discharge treatment of the surface of ultra-high strength polythene (UHSPE). *The 33rd International SAMPE Symposium*, San Diego, California, 1988, (ASME, New York), pp. 254–263.

[29] Holmes S. and Schwartz P. Amination of ultra-high strength polyethylene using ammonia plasma. *Composites Science and Technology* **38** (1990), 1–8.

[30] Li, Z.F. and Netravali A.N. Ammonia plasma treatment of ultra-high strength polyethylene fibres for improved adhesion to epoxy resin, *Journal of Material Science* **27** (1992), 4625–4630.

[31] Vesel A., Junkar I., Cvelver U., Kovac J. and Moretic M., Surface modification of polyester by oxygen- and nitrogen-plasma treatment, *Surface and Interface Analysis* **40** (2008), 1444–1453.

[32] Takemura Y., Yamaguchi N. and Hara T., Study on surface modification of polymer films using atmospheric plasma jet source. *Japanese Journal of Applied Physics* **47** (2008), 5644–5647.

[33] Toosi S., Moradi S., Ebrahimi M. and Hatzikiriakos S.G. Microfabrication of polymeric surfaces with extreme wettability using hot embossing. *Applied Surface Science* **378** (2016), 426–434

[34] Heitz J., Arenholz E., Kefer T., Bäuerle D., Hibst H. and Hagemeyer A. Enhanced adhesion of metal films on PET after UV-laser treatment. *Applied Physics A* **55** (1992), 391–392.

[35] Watanabe H., Shimizu H. and Takata T. Surface change of aramid fiber by laser ablation, *Sen'-i Gakkaishi* **49** (1993), 616–620.

[36] Andrew J.E., Dyer P.E., Forster D. and Key P.H. Direct etching of polymeric materials using a XeCl laser. *Applied Physics Letters* **43** (1983), 717–718.

[37] Breuer J., Metev S. and Sepold G. Photolytic surface modification of polymers with UV-laser radiation. *Journal of Adhesion Science and Technology* **9** (1995), 351–362.

[38] Laurens P., Sadras B., Decobert F., Arefiknonsari F. and Amouroux J. Enhancement of the adhesive bonding properties of PEEK by excimer laser treatment. *International Journal of Adhesion and Adhesives* **18** (1998), 19–27.

[39] Laurens P., Ould Bouali M., Meducin F. and Sadras B. Characterization of modifications of polymer surfaces after excimer laser treatments below the ablation threshold. *Applied Surface Science* **154/155** (2000), 658–663.

[40] Song Q and Netravali A.N. Excimer laser surface modification of ultra-high-strength polyethylene fibers for enhanced adhesion with epoxy resins. Part 1. Effect of laser operating parameters, *Adhesion Science and Technology* **9** (1998), 957–982.

[41] Song Q. and Netravali A.N. Excimer laser surface modification of ultra-high-strength polyethylene fibers for enhanced adhesion with epoxy resins. Part 2. Effect of treatment environment, *Adhesion Science and Technology* **9** (1998), 983–998.

[42] Song Q. and Netravali A.N. Effects of a pulsed XeCl excimer laser on ultra-high strength polyethylene fiber and its interface with epoxy resin, *Journal of Adhesion Science and Technology* **13** (1999), 501–516.

[43] Toosi S.F., Moradi S. and Hatzikiriakos S.G. Fabrication of micro/nano patterns on polymeric substrates using laser ablation methods to control wettability behaviour: A critical review. *Reviews of Adhesion and Adhesives* **5** (2017), 55–78.

[44] Toosi S.F., Moradi S., Kamal S. and Hatzikiriakos S.G. Superhydrophobic laser ablated PTFE substrates, *Journal of Applied Surface Science* **349** (2015), 715–723.

[45] Yoon T.O., Shin H.J., Jeoung S.C. and Park Y-I, Formation of superhydrophobic poly(dimethysiloxane) by ultrafast laser-induced surface modification, *Optics Express* **16** (2008), 12715–12725.

[46] Waugh D.G., Lawrence J. and Shukla P. Modulating the wettability characteristics and bioactivity of polymeric materials using laser surface treatment, *Journal of Laser Applications* **28** (2016), 05002/1–5.

[47] Waugh D.G., Hussain I., Lawrence J., Smith G.C and Toccaceli C. *In vitro* mesenchymal stem cell response to a CO_2 laser modified polymeric material, *Materials Science and Engineering C* **67** (2016) 727–736.

[48] Waugh D.G. and Lawrence J., Laser surface treatments and their effects on adhesion and biomimetic apatite coating formation, *Lasers in Engineering* **390** (2017), 77–95.

[49] Khorasani M.T., Merzedah H. and Sames P.G. Laser induced surface modification of polydimethylsiloxane as a super-hydrophobic material, *Radiation Physics and Chemistry* **47** (1996), 881–888.

[50] Waugh D.G. and Lawrence J. Towards a technique for controlling wettability characteristics and conditioning film formation on polyethylene terephthalate (PET) through laser surface engineering, *Lasers in Engineering* **37** (2017), 207–232.

[51] Lawrence J. and Waugh D.G. CO_2 laser surface engineering of polyethylene terephthalate (PET) for enhanced meat exudate conditioning film formation and bacterial response, *Lasers in Engineering* **38** (2017), 37–56.

[52] Lawrence J. and Li L. Modification of the wettability characteristics of polymethyl methacrylate (PMMA) by means of CO_2, Nd:YAG, excimer and high power diode laser radiation. *Materials Science and Engineering A* **303** (2001), 142–149.

[53] Lawrence J. and Li L., Wettability characteristics of polyethylene (PE) modified with CO_2, Nd:YAG, excimer and high power diode lasers. *Proceedings of the Institution of Mechanical Engineers Part B* **215** (2001), 1735–1744.

[54] Waugh D.G., Avdic D., Woodham K.J. and Lawrence J. Laser surface engineering of polymeric materials and the effects on wettability characteristics. in Mittal K. and Bahners T. (Eds.) *Laser Surface Modification: Relevance to Adhesion,* New York: Scrivener/John Wiley & Sons. 2014.

[55] Waugh D.G. and Lawrence J. On the use of CO_2 laser induced surface patterns to modify the wettability of polymethyl methacrylate (PMMA). *Optics and Lasers in Engineering* **48** (2010), 707–715.

[56] Fowkes F.M. Attractive forces at interfaces. *Industrial & Engineering Chemistry Research* **56** (1964), 40–52.

[57] Owens D.K. and Wendt R.C. Estimation of the surface free energy of polymers. *Journal of Applied Polymer Science* **13** (1969), 1741–1747.

[58] Snakenborg D., Klank H. and Kutter J.P. Microstructure fabrication with a CO_2 laser system. *Journal of Micromechanics and Microengineering* **14** (2003), 182–189.

[59] Dyer P.E., Oldershaw G.A. and Sidhu J. CO_2 laser ablative etching of polyethylene terephthalate. *Applied Physics B* **48** (1989), 489–493.

[60] Beamson G.B. and Briggs D., High resolution XPS of organic polymers: The Scienta ESCA300 database. *Journal of Chemical Education* **70** (1993), A25.

[61] Hawkins W.L., Matreyek W. and Winslow F.H. The morphology of semi crystalline polymers. Pat I. The effect of temperature on the oxidation of ployolefins, *Journal of Polymer Science Part A* **41** (1959), 1–11.

[62] Marechal Ph., Legras R. and Dekoninck J.M. Postcondensation and oxidation processes in molten polyamide 6. *Journal of Polymer Science Part A* **31** (1993), 2057–2067.

[63] Kasahara T., Shoji S. and Mizuno J. Surface modification of polyethylene terephthalate (PET) by 172-nm excimer lamp. *Transactions of The Japan Institute of Electronics Packaging* **5** (2012), 47–53.

[64] Schnabel W. Polymer *Degradation: Principles and Practical Application.* New York: Hanser International. 1981.

[65] Gotoh K., Yasukawa A. and Kobayashi Y. Wettability characteristics of poly(ethylene terephthalate) films treated by atmospheric plasma and ultraviolet excimer light. *Polymer Journal* **43** (2011), 545–551.

[66] Chen Z., Hay J.N. and Jenkins M.J. FTIR spectroscopic analysis of poly(ethylene terephthalate) on crystallization. *European Polymer Journal* **48** (2012), 1586–1610.

[67] Hsu S-T., Tan H. and Yao Y.L. Effect of excimer laser irradiation of biodegradable polymer on its chemical bonding, *The 30th International Congress on Applications of Lasers & Electro-Optics (ICALEO 2011)*, Orlando, Florida, 2011 (LIA, Orlando).

[68] Waugh D.G., Lawrence J., Langer N. and Bidault S. Mixed-State Wetting and Wetting Transitions on Laser Surface Engineered Polymeric Materials, *International Journal of Wettability Science and Technology (IJWST)* **1** (2018), 63–84.

[69] Ueki M., Naka M. and Okamoto I., Wettability of some metals against zirconia coatings, *Journal of Material Science Letters* **5** (1986) 1261–1262.

[70] Li J.G., Microscopic approach of adhesion and wetting of liquid metal on solid ionocovalent oxide surface. *Rare Metals* **12** (1993), 84–96.